P- and PS-wave vector wavefields for anisotropic petrophysics

James Gaiser*
GGC
Del Mar, California USA
Jim@Gaiser-geophysical-consulting.com

SUMMARY

Predicting petrophysical properties of lithology, density and fractures using seismic data is an essential part of reservoir evaluation. In addition to lithology characterization, "frackability" has become a very important area of investigation for high-grading locations for drilling and hydraulic fracture stimulation. Most seismic studies that estimate P- and S-wave impedance, density and brittleness or formation strength use conventional P-wave data and isotropic elastic inversion methods. However, converted-wave (PS-wave) joint inversion and S-wave splitting methods have successfully been used to improve determination of seismic properties for shale plays as well as other unconventional resource plays.

Anisotropic behaviour related to layered media (VTI), fracture properties, stress direction and the geomechanics of shales are increasingly more important for seismic analysis, imaging and reservoir characterization. Vector wavefields are sensitive to these properties and can help identify optimal drilling and stimulation locations. Also, it has been shown that use of conventional elastic parameters for characterizing "brittleness" should include anisotropic corrections to obtain a more accurate response. Including PS-wave seismic data is beneficial for isotropic elastic inversion and should improve anisotropy estimates for identification of potential fracture locations.

Elastic inversion of azimuthally anisotropic amplitude variations (AVAz) is also becoming more important. When layered media are fractured, orthorhombic symmetry of P-wave amplitude depends on S-wave birefringence. PS-waves are ideal for determining this S-wave splitting information from layerstripping and their reflectivity provides additional equations for joint inversion with P-waves. Two coefficients, a radial R_{PSV} and transverse R_{PSH} reinforce anisotropic signatures similar to P-wave reflectivity R_P. Vector wavefields contain all the necessary information for S-wave anisotropy from short wavelength AVAz as well as from long wavelength moveout behaviour.

Key words: Petrophysical properties, vector wavefield, converted waves, anisotropy, joint inversion

INTRODUCTION

The ability to predict how and where fracturing is likely to occur using seismic data has become a very important area of investigation for high-grading locations for drilling and hydraulic fracture stimulation. Often, horizontal well and stimulation programs based on regular patterns are only marginally productive. Identification of "brittleness" and potential fracture locations from seismic data could improve this situation by directing a more targeted drilling program.

Most seismic studies to characterize petrophysical properties and brittleness use conventional P-wave data and elastic inversion methods. Norton et al. (2010) show that conventional seismic methods of amplitude variation with offset or angle (AVO or AVA) inversion and fault mapping can estimate useful elastic properties for predicting geomechanical properties related to stimulation. They observe that hydraulically induced fracture networks prefer lower Poisson's ratio (PR) or lower V_P/V_S ratio rock in the Montney shale in NE Canada. Also, there appears to be a lack of microseismic events in the vicinity of secondary faults.

Gray (2012) uses P-wave 3D wide-angle, wide-azimuth data to compute Young's modulus E and Poisson's ratio ν to predict the differential horizontal stress ratio (DHSR) in the Colorado shale in Alberta, Canada. The ratio $(\sigma_H-\sigma_h)/\sigma_h$ can be estimated from azimuthal AVA (AVAz) inversion, where σ_H and σ_h are the maximum and minimum horizontal stresses, respectively, and is a function of E and ν. The azimuthal anisotropic behaviour of DHSR is an indication of how the reservoir is likely to fracture. Also, he suggests that both wide-angle, wide-azimuth, conventional 3D P-wave data, and multi-component converted wave (PS-wave) seismic data should allow the estimation of these parameters.

PS-wave joint inversion and S-wave splitting methods have successfully been used to determine elastic properties (Dariu et al., 2003). In the Junggar basin in northwestern China, Dang et al. (2010) computed the V_P/V_S impedance ratio, fluid factor, and Poisson's ratio to explain differences between productive and nonproductive wells. Bale et al. (2012) investigate S-wave birefringence properties as a baseline survey to monitor the toe-to-heel air-injection (THAI) process at Kerrobert field in western Saskatchewan. This is a heavy oil prospect where a burn front is maintained to lower the viscosity of oil. A10% S-wave splitting anisotropy anomaly over the time window of the reservoir is located at the two longest operating air injectors in the field.

Chaveste et al. (2013) estimate rock properties through P-and PS joint inversion from the Marcellus shale in Pennsylvania. They illustrate the potential risk reduction in qualitative estimation of total organic content (TOC) and fracture characterization. Joint inversion provides better estimates of both shear-wave velocity V_S and density ρ than P-wave inversion alone, as calibrated with log data. Here, density is inversely proportional to the gamma-ray log, which is indicative of TOC. Barnola and Ibram (2014) demonstrate similar joint inversion benefits for estimating S-wave impedance and density at the Schiehallion field, United Kingdom continental shelf.

Also, Grossman et al. (2013) conduct a study of Pouce Coupe field time-lapse multicomponent surveys investigating two horizontal well hydraulic stimulations of the Montney shale. S-wave splitting layer stripping analyses show a strong correlation between the magnitude and orientation of seismically derived induced reservoir birefringence and individual stage production. This is based on a comparison of spinner production data with increases in S-wave splitting near hydraulically stimulated horizontal wells.

In this paper, I extend Jílek's (2002) approximations of PS-wave reflectivity in azimuthally anisotropic media. These include higher order coefficients in the vertical angle of incidence for PS-wave radial and transverse reflection coefficients, R_{PSV} and R_{PSH}, respectively. I demonstrate with synthetic and field data that R_{PSV} and R_{PSH} are routinely observed during conventional PS-wave processing for the S-wave splitting parameter $\Delta\gamma^{(S)}$. Also, I model amplitudes for orthorhombic media where fracture direction can change across the interface. These anisotropic behaviours of PS-wave are in principle available for joint inversion with P-waves to help characterize the petrophysics of reservoirs as well as other lithologies for unconventional shale plays. Inverting for such complex velocity models however may require different approaches than conventional joint AVAz methods.

ANISOTROPIC ELASTIC PARAMETERS

Goodway et al. (2010) discuss the anisotropy related to minimum closure stress in terms of $\gamma^{(S)}$. Later, Hu et al. (2015) relate similar concepts of pressure (stress) gradient to ε and δ. However, Thomsen (2013) has emphasized the importance of vertical polar anisotropy (VPA aka VTI) when estimating conventional elastic parameters such as incompressibility K, E and ν, and even the Lamé parameters λ and μ for characterizing frackability or brittleness. These elastic parameters depend on the anisotropy terms, ε, δ, and γ in various forms. He shows that the bulk modulus K can be expressed as,

$$K \approx K_0 + \frac{8}{9}\left[M_0\varepsilon + \frac{M_0}{2}\delta_w - \mu_0\gamma \right] \tag{1}$$

using perturbation theory, where K_0 is the incompressibility of an equivalent medium with the vertical P-wave modulus $M_0=\lambda_0+2\mu_0$, and μ_0 is likewise the vertical S-wave modulus of rigidity. Here, δ_w is the linear, weak anisotropy approximation of δ. Thus, estimates of K from conventional inversions of K_0 will result in errors if the anisotropy is not included.

Thomsen (2013) also derives similar forms for Young's moduli E_{33} and E_{11} in the vertical and horizontal directions, respectively, and Poisson's ratios ν_{13} and ν_{12} in the vertical and horizontal off-axis directions, respectively. However, these are unintuitive, complicated expressions more suited for engineering applications since they are both related to strains (displacements) without confining stresses. Although their state of stress is not consistent with the state of stress and strain within P- or S-wavefields, they all have contributions from ε, δ_w, and γ that should be included for proper evaluation. The elastic properties associated with wavefields are λ and μ. The off-axis anisotropic forms are given by,

$$\lambda_{12} = \lambda_0 + 2M_0\varepsilon - 4\mu_0\gamma \tag{2}$$

and

$$\lambda_{13} = \lambda_0 + 2M_0\delta_w, \tag{3}$$

as the stress-strain ratios of a P-wave traveling in the horizontal x_1 direction with particle motion (strain) only in that direction. Equation (3) arises from the linearized definition of δ and is also the vertical off-axis elastic parameter. The on-axis Lamé parameters in a VPA medium can be identified as, $\lambda_{33}=\lambda_0$ and $\lambda_{11}=\lambda_{12}$ in the vertical and horizontal directions, respectively, and $\mu_{55}=\mu_0$ and $\mu_{66}=\mu_{55}(1+2\gamma)$.

However, the challenge is estimating these anisotropic properties accurately enough from P-wave data. Lin and Thomsen (2013) obtain an estimation of δ using well log derived isotropic synthetic data. They compute the difference with CDP gathers at the well, assuming a VPA R_P reflection coefficient response (Rüger, 1998),

$$R_P(\theta) \cong R_0 + R_2\sin^2\theta + R_4\sin^2\theta\tan^2\theta \tag{4}$$

where θ is the angle of incidence and the coefficients are:

$$\begin{aligned} R_0 &= \frac{1}{2}\frac{\Delta Z}{\overline{Z}} = \frac{1}{2}\left[\frac{\Delta V_{P0}}{\overline{V}_{P0}} + \frac{\Delta\rho}{\overline{\rho}} \right], \\ R_2 &= \frac{1}{2}\left[\frac{\Delta V_{P0}}{\overline{V}_{P0}} - \left(\frac{2\overline{V}_{S0}}{\overline{V}_{P0}} \right)^2 \frac{\Delta\mu_0}{\overline{\mu}_0} + \Delta\delta_w \right], \\ R_4 &= \frac{1}{2}\left[\frac{\Delta V_{P0}}{\overline{V}_{P0}} + \Delta\varepsilon \right]. \end{aligned} \tag{5}$$

They obtain δs that correlate with the gamma-ray log in a long wavelength behaviour. Also, they indicate that the ε parameter in coefficient R_4 could be estimated in a similar manner from far offset data.

Vasconcelos and Grechka (2007) invert for all the anisotropic parameters from multicomponent NMO data for fracture properties in the Mesaverde tight gas sands. They use 9C horizontal vibrator data that is typically not available in practice. However, Grechka et al. (1999) have shown with physical model data that $\gamma^{(1)}$ and $\gamma^{(2)}$ can also be determined from PS-wave NMO in orthorhombic media. This is possible by taking advantage of the known (elliptical) azimuthal NMO-velocity function, despite the fact that PSH-waves are not created in the two vertical symmetry planes. Their NMO signatures can be reconstructed from the moveout measured on PSH-like reflections in azimuths near these symmetry planes.

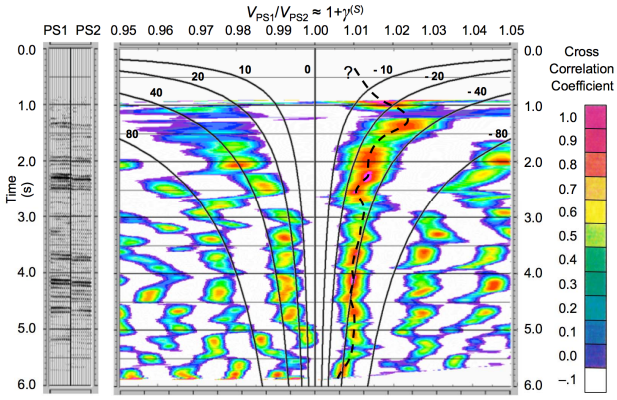

Figure 1: Average velocity ratio analysis between the fast PS1 and slow PS2 reflection stacks (left) before S-wave splitting corrections. Contours indicate constant PS2 time delays (ms) and the dashed line shows the picked relationship between the split S-waves. From Gaiser and Van Dok (2001).

S-wave splitting analyses of PS-wave data can also provide information about γ. However, this is for the S-wave splitting parameter $\gamma^{(S)}$ given by Tsvankin (1997),

$$\gamma^{(S)} \equiv \frac{\mu_{44}-\mu_{55}}{2\mu_{55}} = \frac{\gamma^{(1)}-\gamma^{(2)}}{1+2\gamma^{(2)}} \approx \frac{V_{S1}-V_{S2}}{V_{S2}} \approx \frac{t_{S2}-t_{S1}}{t_{S1}} \tag{6}$$

where $\mu_{44} \neq \mu_{55}$ in orthorhombic media, V_{S1} and V_{S2} are the S-wave fast and slow vertical velocities, and t_{S2} and t_{S1} are the S-wave vertical traveltimes of the slow and fast wave, respectively. Superscripts correspond to the two vertical symmetry planes where fractures are in the $[x_2, x_3]$ or $[y, z]$ vertical plane and fracture normal points in the x_1 or x direction. Figure 1 shows long wavelength estimates of average $\gamma^{(S)}$ obtained by cross correlation of fast and slow PS-wave reflection stacks before correcting for S-wave splitting (Gaiser and Van Dok, 2001). A dashed line indicates the $\gamma^{(S)}$ function picked on the maximum cross-correlation values. Variations with respect to contours of S-wave split splitting delays identify intervals where birefringence changes in two-way time. This is based on the assumption that symmetry plane orientation does not change with depth.

AZIMUTHAL AVA CHALLENGES

Anisotropic behaviour of AVAz is also desirable for elastic inversions. In orthorhombic media, Rüger (1998) derives P-wave AVA in principal symmetry planes, and shows that the $\sin^2\theta$ gradient term for R_P reflection coefficients in the $[x_1, x_3]$ plane becomes,

$$R_2^{[x_1,x_3]} = \frac{1}{2}\left[\frac{\Delta V_{P0}}{\overline{V}_{P0}} - \left(\frac{2\overline{V}_{S0}}{\overline{V}_{P0}}\right)^2\left(\frac{\Delta\mu_0}{\overline{\mu}_0} - 2\Delta\gamma^{(S)}\right) + \Delta\delta_w^{(2)}\right], \tag{7}$$

where it depends on contrasts in both $\Delta\delta^{(2)}$ in the x_2 symmetry plane, and $\Delta\gamma^{(S)}$ the S-wave splitting anisotropy. In this case, V_{S0} and μ_0 correspond to the fast vertical S-wave velocity and modulus, respectively. This indicates that it might be difficult to distinguish the two responses during inversion. Also, the difference in anisotropic reflectivity between the two principal directions is,

$$R_P^{[x_1,x_3]} - R_P^{[x_2,x_3]} = \left[\left(\frac{2\overline{V}_{S0}}{\overline{V}_{P0}}\right)^2 2\Delta\gamma^{(S)} - \frac{1}{2}\left(\Delta\delta_w^{(2)} - \Delta\delta_w^{(1)}\right)\right]\sin^2\theta + \frac{1}{2}\left[\Delta\varepsilon^{(2)} - \Delta\varepsilon^{(1)}\right]\sin^2\theta\tan^2\theta \tag{8}$$

resulting in a third order difference in elastic parameters of $\Delta\delta^{(2)}$–$\Delta\delta^{(1)}$ and the $\Delta\varepsilon^{(2)}$–$\Delta\varepsilon^{(1)}$, but only a second order difference from $\Delta\gamma^{(S)}$ for the S-wave contribution. This S-wave splitting term is essentially proportional to the contrast in $[(V_{S1}-V_{S2})/V_{S2}]$ in terms of the vertical shear velocities (typically 5±3%) and may have a larger contribution to the anisotropy of the P-wave AVA gradient. Recently, Mahmoudian et al. (2015) investigate a physical model with orthorhombic symmetry for P-wave AVAz. Their results suggest that the $\Delta\gamma^{(S)}$ might be able to be determined from the $\sin^2\theta$ gradient in field data.

An additional source for this birefringence parameter is from PS-waves. Jílek (2002) has shown that in azimuthally anisotropic media, both radial R_{PSV} and transverse R_{PSH} reflection coefficients exist. Expanding to 3rd order in $\sin^3\theta$ results in reflection coefficients for the radial,

$$\begin{aligned} R_{PSV}(\phi,\theta) \approx & -A_{iso}\left(\Delta\rho,\Delta\beta\right)\sin\theta + B_{iso}\left(\Delta\rho,\Delta\beta\right)\sin^3\theta \\ & -\left[A_{ani}^{(1)}\left(\phi,\Delta\gamma^{(S)},\Delta\delta^{(2)}\right) + A_{ani}^{(2)}\left(\phi,\Delta\delta^{(2)}\right)\right]\sin\theta \\ & -\left[B_{ani}^{(1)}\left(\phi,\Delta\gamma^{(S)},\Delta\delta^{(2)}\right) + B_{ani}^{(2)}\left(\phi,\Delta\delta^{(2)}\right)\right]\sin^3\theta \end{aligned} \tag{9}$$

that have a similar form as R_P with respect to the contrasts in anisotropic terms as compared to equation (7), where superscripts correspond to the symmetry planes. There is a third group of coefficients in equation (9) for $\sin^3\theta$ not shown. These depend on large

angle of incidence contrasts in $\Delta\varepsilon^{(1)}$ and $\Delta\varepsilon^{(2)}$, and $\Delta\delta^{(3)}$ the off-axis anisotropy in the horizontal symmetry plane. The transverse reflection coefficient is,

$$R_{PSH}(\phi,\theta) \approx -D_{ani}^{(1)}\left(2\phi, \Delta\gamma^{(S)}, \Delta\delta^{(2)}-\Delta\delta^{(1)}\right)\sin\theta+E_{ani}^{(1)}\left(2\phi, \Delta\gamma^{(S)}, \Delta\delta^{(2)}-\Delta\delta^{(1)}\right)\sin^3\theta \quad (10)$$

where there are no isotropic terms. This provides interesting insights to the signature of R_{PSH} where it has a similar form as equation (8) and 2ϕ angular dependence with azimuth (Gaiser, 2014). There is a similar group of coefficients not shown in equation (10) for $\sin^3\theta$ that depend on $\Delta\varepsilon^{(1)}$ and $\Delta\varepsilon^{(2)}$, and $\Delta\delta^{(3)}$.

AVAz displays in Figure 2 show that R_{PSH} can have amplitudes about a quarter of R_{PSV}. The contrasts used for splitting are 5% and there is a –40° change in the fracture orientation between the incident and reflecting media. Note that this shifts the null amplitude azimuth of R_{PSH} in the positive azimuth direction. Contrasts in the other elastic parameters around 5%, are from Jílek (2002).

These reflectivities should provide additional equations for joint inversion with P-waves. R_{PSV} reinforces S-wave and anisotropy behaviour similar to R_P and the R_{PSH} reflectivity contributes entirely to the anisotropy. Although most PS-wave reflection amplitude exhibits interference phenomena from S-wave splitting, R_{PSV} and R_{PSH} are routinely observed after layerstripping has removed the propagation effects of birefringence in field and synthetic data (not shown here).

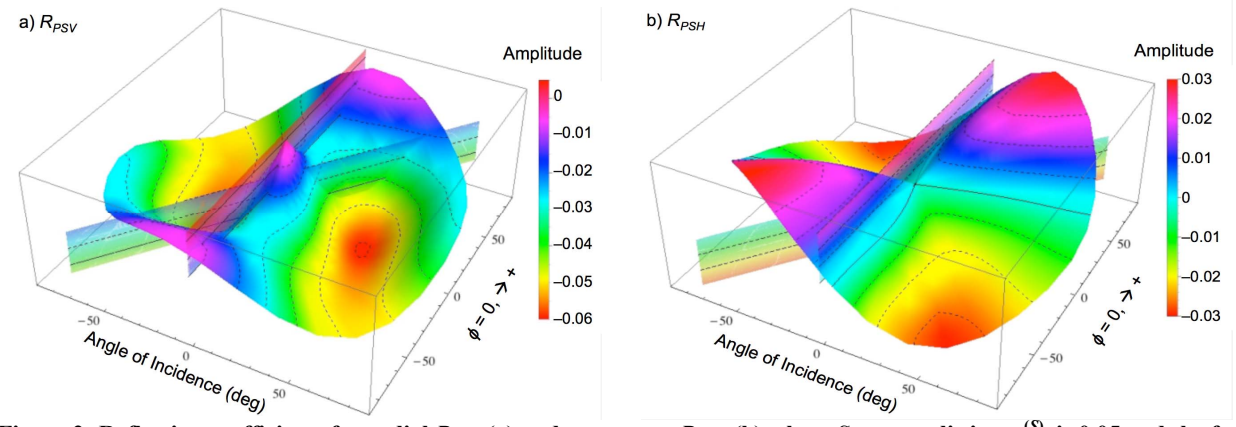

Figure 2: Reflection coefficients for radial R_{PSV} (a) and transverse R_{PSH} (b) where S-wave splitting, $\gamma^{(S)}$, is 0.05 and the fracture direction changes by –40° in the lower medium. The vertical axis is proportional to amplitude but also represents depth of the two fracture planes. Dashed contours are 0.01, and the null amplitude contours of R_{PSH} are twisted off axis about +15° in azimuth and are not aligned with the fracture direction at 90° in the upper medium.

Figure 3 shows an example of this on radial and transverse, common-azimuth-stack traces from the Gulf of Mexico. In 3a the data before layerstripping show little to no azimuthal variation in traveltime for early reflections on the radial component (polarized in the source-receiver direction), but later in two-way time reflections exhibit a sinusoid-like signature (1.5 seconds) and eventually the fast and slow S-waves separate completely (after 2.0 seconds). On the transverse component there is a clear 2ϕ azimuthal response with polarity reversals every 90 degrees.

Figure 3b shows the data after layerstripping to 1.5 seconds. Vertical lines indicate the principal azimuths of the fast (solid) and slow (dashed) symmetry planes determined by the analysis. Reflections are aligned on the radial and amplitude to 1.5 seconds represent R_{PSV}, and residual amplitude on the transverse component represents R_{PSH} (Gaiser, 2014). After 1.5 seconds there is clear S-wave splitting behaviour indicating that further layerstripping is needed. In terms of AVAz it is important to understand that the two components in Figure 3b are a close approximation to the $\sin\theta$ coefficients in equations (9) and (10). Indicated in the circles is an example where amplitude null directions do not agree with principal directions determined by travel times. This suggests a change in the principal directions across the interface.

DISCUSSION

All the necessary information to obtain γ is available from P- and PS-waves by combining NMO and AVA analysis (Rüger, 1998). NMO velocities can be determined from P-waves to obtain azimuthal variation of δ and $\eta=(\varepsilon-\delta)/(1+2\delta)$. Cho et al. (2015) perform accurate moveout analyses for S-wave anisotropy estimates via azimuthal AVAz inversion. Also, V_{PSV1} and V_{PSV2} as well as for V_{PSH} can be determined from converted wave data (Grechka et al., 1999). Layer stripping provides $\Delta\gamma^{(S)}$ from S-wave splitting traveltimes, orientation to the principal axes, and also R_{PSV} and R_{PSH} reflectivity.

Registration with P-wave gives V_P/V_{S1} and V_P/V_{S2} and aligns the wavefields for joint AVAz inversion for obtaining elastic properties and anisotropy. However, joint inversion of P- and PS-wave data in a full-waveform method without prior registration (Roure et al., 2015) may actually be the optimal approach. This can be accomplished in a multistep process (Li and Mallick, 2015). First, isotropic petrophysical properties are determined from joint inversion of stable near-offset data that is independent of azimuth. Second, the anisotropic parameters in equations (7) and (8) can be determined in the principal symmetry axes.

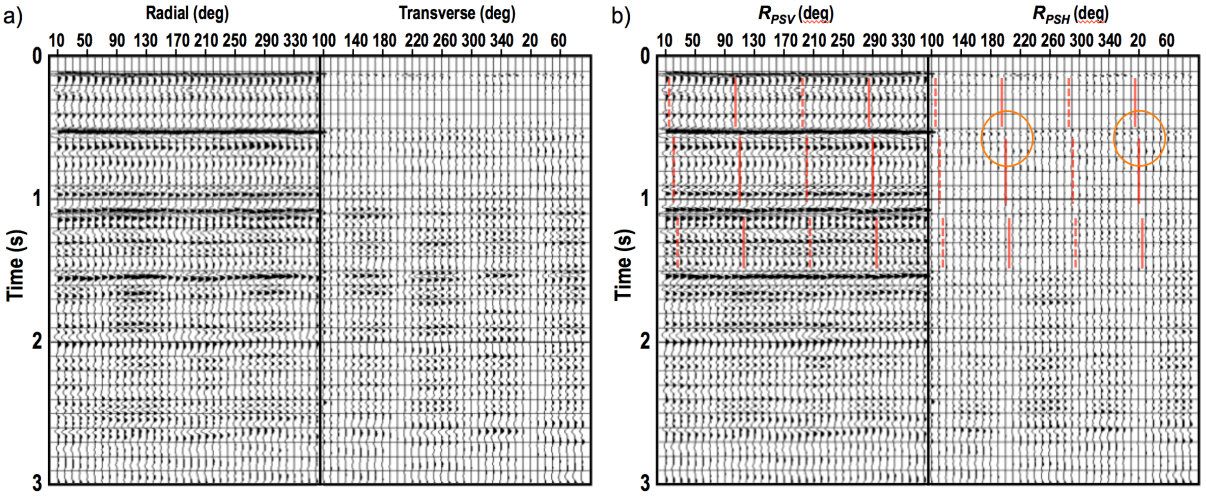

Figure 3: Common receiver gathers where each trace is a common azimuth stack of radial and transverse PS-wave data before (a) and after (b) layerstripping. Reflection amplitude in a) is a combination of reflection coefficients and interference effects of S-wave splitting. After correcting for birefringence to 1.5 seconds, reflection amplitude is an estimate of reflection coefficients R_{PSV} and R_{PSH}. From Gaiser (2014).

CONCLUSIONS

Anisotropic elastic parameters can help describe petrophysical properties related to lithology, brittleness, and fractures/stresses. Vector wavefields that include PS-waves improve S-wave impedance and density estimates by joint inversions with P-waves. Thus, a full wavefield joint AVAz inversion should also help constrain anisotropic elastic parameters of ε, δ, and γ in a similar manner. In addition to providing the anisotropic behaviour for shales and other lithologies, the azimuthal property of $\gamma^{(S)}$ gives an estimate of crack density.

ACKNOWLEDGMENTS

I thank Petr Jílek and Ilya Tsvankin for very interesting and helpful discussions, and CGG for permission to publish this material.

REFERENCES

Bale, R., T. Marchand, K. Wilkinson, K. Wikel and R. Kendall, 2012, Processing 3-C heavy oil data for shallow shear-wave splitting properties: methods and case study: CSEG Recorder, **37**, no. 5, 24–32.

Barnola, A.S. and M. Ibram, 2014, 3D simultaneous joint PP-PS prestack seismic inversion at Schiehallion field, United Kingdom continental shelf: Geophysical Prospecting, **62**, no. 2, 278–292.

Chaveste, A., Z. Zhao, S. Altan, and J. Gaiser, 2013, Robust rock properties through PP-PS processing and interpretation – Marcellus shale: The Leading Edge, **32** (1), 86–92.

Cho, D., D. Miller, M. Norton, A. Kumar Dey and F. Kierulf, 2015, Shear wave anisotropy estimates via azimuthal amplitude-variation-with-offset inversion: CSEG Recorder, **40**, no. 6, 32–36.

Dang, Y., B. Lou, X. Miao, P. Wang, S. Zhang and L. Shen, 2010, Delineating oil-sand reservoirs with high-resolution PP/PS processing and joint inversion in the Junggar Basin, Northwest China: The Leading Edge, **29**, no. 10, 1212–1219.

Dariu, H., P.Y. Granger, J.P. Fjellanger and P. Riste, 2003, Multicomponent AVO inversion using simulated annealing: 65th Conference and Technical Exhibition, EAGE, Extended Abstract D16, 1–5.

Gaiser, J., 2014, Challenges for PS-wave inversion in azimuthally anisotropic media: 16th International Workshop on Seismic Anisotropy, Natal, Brazil.

Gaiser, J. and R. Van Dok, 2001, Green River basin 3D/3C case study for fracture characterization: analysis of PS-wave birefringence: 71st Annual International Meeting, SEG, Expanded Abstract, MC1.1, 764–767.

Goodway, B., M. Perez, J. Varsek and C. Abaco, 2010, Seismic Petrophysics and isotropic-anisotropic AVO methods for unconventional gas exploration: The Leading Edge, **29** (12), 1500–1508.

Gray, D., P. Anderson, J. Logel, F. Delbecq, D. Schmidt, and R. Schmid, 2012, Estimation of stress and geomechanical properties using 3D seismic data: First Break, **30** (3), 59–68.

Grechka, V., S. Theophanis, and I. Tsvankin, 1999, Joint inversion of P- and PS-wave in orthorhombic media: theory and a physical modeling study: Geophysics, **64** (1), 146–161.

Grossman, J.P., G. Popov, and C. Steinhoff, 2013, Integration of multicomponent time-lapse processing and interpretation: focus on shear-wave splitting analysis: The Leading Edge, **32** (1), 32–38.

Hu, R., L. Vernik, L. Nayvelt and A. Dicman, 2015, Seismic inversion for organic richness and fracture gradient in unconventional reservoirs: Eagle Ford shale, Texas: The Leading Edge, **34** (1), 80–84.

Jílek, P., 2002, Modeling and inversion of converted PS-wave reflection coefficients in anisotropic media: a tool for quantitative AVO analysis: Colorado School of mines, Doctoral Thesis CWP 400.

Lin, R. and L. Thomsen, 2013, Extracting polar anisotropy parameters from seismic data and well logs: 83rd Annual International Meeting, SEG, Expanded Abstract, ANI-1.6, 310–314.

Li, T. and S. Mallick, 2015, Multicomponent, multi-azimuth pre-stack seismic waveform inversion for azimuthally anisotropic media using a parallel and computationally efficient non-dominated sorting genetic algorithm: Geophysical Journal International, **200**, no. 2, 1134–1152.

Mahmoudian, F., G.F. Margrave, J. Wong, and D.C. Henley, 2015, Azimuthal amplitude variation with offset analysis of physical modeling data acquired over an azimuthally anisotropic medium: Geophysics, **80** (1), C21-C35.

Norton, M, W. Hovdebo, D. Cho, M. Jones, and S. Maxwell, 2010, Surface seismic to microseismic: an integrated case study from exploration to completion in the Montney shale of NE British Columbia, Canada, 80th Annual International Meeting, SEG, Expanded Abstract, PSC 2.2, 2095–2099.

Roure, B., V. Souvannavong, J.P. Coulon and D. Hampson, 2015, Joint PP-PS inversion without prior data registration: 77th Conference and Technical Exhibition, EAGE, Extended Abstract Tu-N116-04, 1–5.

Rüger, A., 1998, Variation of P-wave reflectivity with offset and azimuth in anisotropic media: Geophysics, **63** (3), 935–947.

Thomsen, L., 2013, On the use of isotropic parameters λ, E, ν, K to understand anisotropic shale behavior: 83rd Ann. Internat. Mtg., SEG, Exp. Abs. ANI-1.8, 320–324.

Tsvankin, I., 1997, Anisotropic parameters and P-wave velocity for orthorhombic media: Geophysics, **62** (4), 1292–1309.

Vasconcelos, I. and V. Grechka, 2007, Seismic characterization of multiple fracture sets at Rulison field, Colorado: Geophysics, **72** (2), B19–B30.